DOI 10.31489/2022No3/10-17

UDC 534.16, 536.21, 537.322, 537.323, 548.1.024

SEVERAL NOTES ON THE LATTICE THERMAL CONDUCTIVITY OF FRACTAL-SHAPED NANOPARTICLES

Shishulin A.V.[1,2]*, Potapov A.A.[3,4], Shishulina A.V.[5,6]

[1]Pleiades Publ., Ltd., Moscow, Russia, chichouline_alex@live.ru
[2]G.A. Razuvaev institute of organometallic chemistry, Russian Academy of sciences, Nizhny Novgorod, Russia
[3]V.A. Kotel'nikov institute of radio engineering and electronics, Russian Academy of sciences, Moscow, Russia
[4]JNU-IREE RAS Joint Laboratory of Information Technology and Fractal Processing of Signals, Jinan University, Guangzhou, China
[5]R.E. Alekseev Nizhny Novgorod State technical University, Nizhny Novgorod, Russia
[6]N.I. Lobachevsky Nizhny Novgorod State University, Nizhny Novgorod, Russia

Using the additive technologies in the production of nanoparticle-fabricated three-dimensional materials has become one of the most promising ways of obtaining effective and low-cost thermoelectric energy converters. Nanostructuring provides a route to modifying selectively the transport properties which determine the materials thermoelectric efficiency. In this paper, we have shown one more effect which consists in a significant dependence of the contribution of lattice vibrations to the thermal conductivity coefficient of a nanoparticle (its reducing is required in practice) on its morphology for nanoparticles of a pure substance. The particle morphology has been specified by the values of its effective diameter, fractal dimension and surface roughness.Using nanoparticles of pure bismuth at low temperatures as an example, we have demonstrated a notable decrease in the lattice thermal conductivity in "complicating" the particle morphology. In the final section, we have presented methods of calculating characteristics of nanoparticle ensembles, the methodology of measuring the fractal dimension experimentally also being discussed.

Keywords: thermoelectric materials, thermal conductivity, nanoparticles,phonons, fractal dimension.

Introduction

Thermoelectric materials and energy converters on their basis have been an object of considerable interest among researchers in recent years [1]. The expanding field of their application includes energy generators which operate in extreme conditions (radioisotope thermoelectric generators for Voyager-2 and other space modules [1]), thermoelectric converters for utilizing the waste heat dispersed into environment [2], cooling and temperature-control facilities based on the Peltier effect, etc. [3]. Despite the intensive development of multiple approaches to obtain thermoelectric materials with promising properties based on low-dimension structures (nanofilms [4,5], quantum wires [6], etc.), highly-effective and low-cost thermoelectrics can be produced on the basis of 3D nanocrystalline structures [7,8]. The scheme which illustrates the performance of a typical thermoelectric converter is given in Fig. 1.

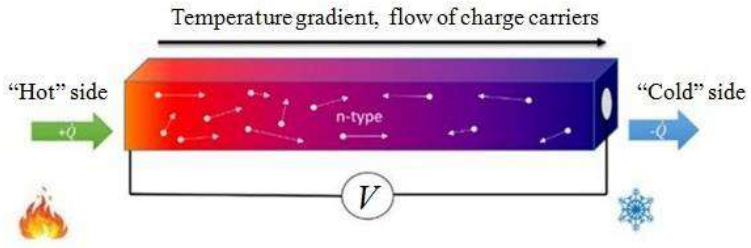

Fig.1. Schematic illustration of the performance of a typical thermoelectric converter. A thermoelectric device creates a voltage when there is a different temperature on each size of a thermoelectric material sample. At the atomic scale, an applied temperature gradient causes charge carriers in the material to diffuse from the "hot" side to the "cold" side.

The key characteristic parameter determining the materials thermoelectric efficiency is the dimensionless figure of merit, *ZT*, which can be expressed as a function of thermal conductivity κ, electrical conductivity σ and Seebeck coefficient α: $ZT = \alpha^2 \sigma \overline{T} / \kappa$ where $\overline{T}$ is the average temperature between the "hot" and "cold" sides of a thermoelectric converter and $\kappa \approx \kappa_{car} + \kappa_{ph}$ [1,2,7]. Here, κ_{car} and κ_{ph} are the contributions of charge carriers (electrons, holes) and phonons (crystal lattice vibrations) to the thermal conductivity, respectively (several other contributions, e.g. the ones of excitons or spin-orbit coupling, are neglected, being much lower). In every single material, as a rule, electrical conductivity σ and the contribution of carriers to the total thermal conductivity, κ_{car}, cannot be varied separately, and optimal thermoelectric properties can be obtained primarily through the reduction of the phonon contribution κ_{ph}. In nanostructured polycrystalline materials, κ_{ph} is generally decreased through the formation of multiple interfaces (grain boundaries) which scatter thermal phonons [9], add to this, the energy filtration of charge carriers at grain boundaries, which reduces the contribution of low-energy carriers to transport properties, results in an additional increase in the Seebeck coefficient [2]. Nanostructured polycrystalline thermoelectric materials can be produced using various technologies of up-to-date powder metallurgy, e.g. spark plasma sintering, selective laser sintering, selective laser melting, etc. [7,8].

It is necessary to mention that several effects manifesting themselves at the nanoscale provide additional "knobs" which allow tuning the properties of thermoelectric materials. For example, the phase equilibria in small-volume particles of stratifying solutions become morphology-dependent, being different from the ones of macroscopic-sized structures, which leads to the possibility of the formation of stable phases, the compositions of which are highly unstable in macroscale particles at the operation temperatures. As we have previously shown in [10,11] using the combination of thermodynamic [12] and *ab initio* [13] approaches, such phases correspond to much lower values of the phonon thermal conductivity coefficients favoring the growth of the thermoelectric figure of merit; we have also predicted the set of optimal morphological characteristics (as well as some other factors) which lead to reaching the minimum value of κ_{ph}. These effects have been interpreted as the implementation of several mechanisms of lowering the free energy of a nanoscale system, which can also be competitive in several cases leading to specific non-monotonous dependences of phase equilibria characteristics [14]. Despite the fact these effects are realized at the nanoscale particle sizes (available for the additive technologies, however) in the majority of cases, there is a broad class of systems with greater molecular masses in which such effects manifest themselves at characteristic sizes even several thousand times higher [15,16] (and should probably be called "small-amounts-of-matter effects" instead of "size effects" [17]).

In the present paper, we have shown for the first time another specific effect, which consists in additional decrease in the phonon contribution to the thermal conductivity coefficient, manifesting itself in nanoparticles even of pure substance. Physically, this effect is associated with an increase in the morphology-dependent fraction of surface atoms which have oscillation characteristics being different from the ones of atoms in the particle volume. The dependence of κ_{ph} on particle morphology has been constructed using nanoparticles of pure bismuth as an example. Bismuth (being either pure or alloyed with antimony) is considered to be one of the most efficient thermoelectric materials especially at low temperatures with a large set of possible application fields including space technologies. The obtained estimates combined with the ones in [10] show one more possible route to the more effective optimization of the thermoelectric performance of particle-fabricated nanoalloys.

1. Lattice thermal conductivity of nanoscale particles: the morphology matters

The specific properties of the substance in systems of a very small volume have been investigated by the scientific community since 1850: M. Faraday was the first to emit the idea that the melting temperature of extremely tiny particles should be smaller than the one for the bulk state [18]. A detailed review concerning unique properties of the substance at the nanoscale including the melting behavior can be found in Refs [18,19]. Here, in order to determine the morphology-dependent melting temperature of nanoparticles, we have used the model suggested by W.H. Qi and M.P. Wang [20]. Being experimentally verified for nanoparticles of pure bismuth, this model is based on the considerations of J.H. Rose *etal*. [21,22] on the

binding theory of solids which allow deriving the well-known empirical relation between melting temperature T_m and cohesive energy E_{coh} for pure metals: $T_m = 0.032E_{coh}/k_B$ where k_B is the Boltzmann constant. According to the approach of W.H. Qi and M.P. Wang, the dependence of the nanoparticle melting temperature on the morphology can be described by the following equation: $T_m^{nano} = T_m^{bulk}\left(1 - 6kr_{at}/d_{eff}\right)$ where T_m^{nano} and T_m^{bulk} are the melting temperatures of a nanoparticle and the bulk material, respectively, r_{at} is the atomic radius and k and d_{eff} are the shape coefficient and the effective diameter of a nanoparticle (the diameter of a spherical nanoparticle of the same volume). The shape coefficient is the ratio between the surface area of the particle under consideration, A, and the surface area of the sphere of the same volume, A_0: $k = A/A_0$ (in details, such approach and its variants have been described in [12,23,24]). High values of shape coefficient *k* could be obtained, for example, in the case when the considered particles have the shapes similar to simple non-spherical geometric structures (for example, *k*=1.49 for a tetrahedron, *k*=1.52 for a cone, *k*=3.20 for a star icosahedron (an icosahedron with a tetrahedron at each face)) or structures extended in one direction (for example, values *k*>2.00 correspond to oblate spheroids with aspect ratio *a*/*b*>5 or to prolate spheroids with *a*/*b*>3). Moreover, high surface-to-volume ratios are also characteristic for particles of complicated and irregular shapes, in order to take into account their morphology, the notion of fractal geometry is often used [25]. According to the approach suggested by us in [26,27], the shape of a particle can be characterized by its fractal dimension *D* which correlates its volume *V* and surface area *A*: $A = CV^{2/D}$ where *C* is a numerical coefficient. For real irregular morphologies of materials structure elements, *D*<3 and is typically non-integer. The most classic examples of fractal structures are *worm-like*, *amoeba-like*, and *porcupine-like* ones [26] (see Fig. 2a). The formation of fractal-shaped structures is generic for many non-equilibrium processes [28].

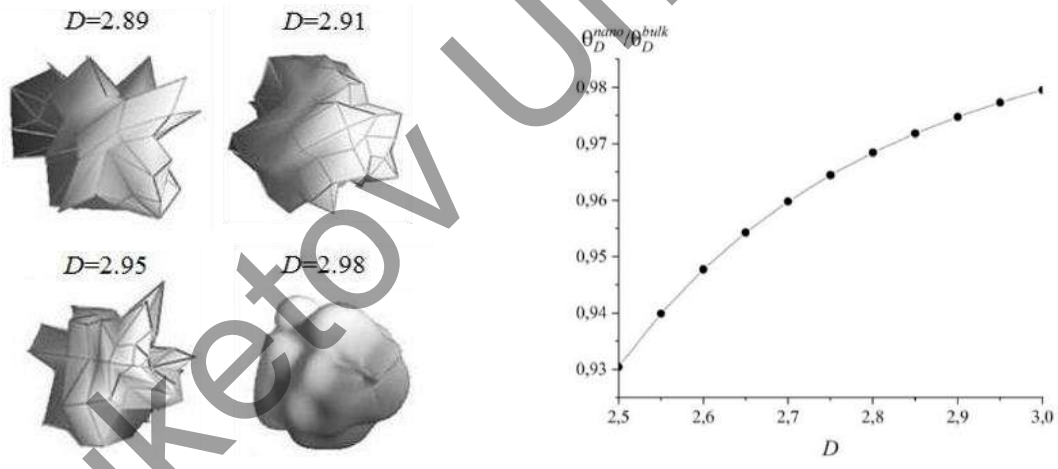

a *b*

Fig 2. a) examples of "amoeba-like" and porcupine-like" fractal structures with various *D*; b) the dependence of relative Debye temperature $\theta_D^{nano}/\theta_D^{bulk}$ on the fractal dimension for a nanoparticle with d_{eff}=40 nm.

Melting temperature and temperature θ_D, at which all the modes of oscillations in the considered solid medium become excited (known as the Debye temperature), are interrelated according to the Lindemann criterion of melting [29]. This criterion is based on the statement that the root-mean-square amplitude of thermal oscillations at this temperature reaches a certain critical value which represents a constant fraction of the characteristic interatomic distance, δ_L, in the crystal lattice. δ_L is the so-called "Lindemann parameter", $\delta_L \in [0.15, 0.30]$. The Lindemann criterion can be mathematically formulated as follows [29]: $T_m = 4\pi^2 A\delta_L^2 a^2 k_B \theta_D / 4N_A h^2$ where h is the Planck constant, a is the characteristic interatomic distance and A is the molar mass of the considered substance. Since the characteristic distances in the crystal lattice are independent on the size and shape of a particle when the particle size does not exceed several nanometers,

we obtain $\theta_D \sim T_m^{1/2}$, $\theta_D^{nano} = \theta_D^{bulk}\left(1-6kr_{at}/d_{eff}\right)^{1/2}$ while shape coefficient k is expressed is a function of volume V, $V=\pi d_{eff}^3/6$, and fractal dimension D of a nanoparticle: $k(V,D)=V^{2/D}/\left(3V/4\pi\right)^{2/3}$. The dependence of temperature θ_D on the fractal dimension for a nanoparticle with d_{eff}=40 nm is plotted in Fig. 2b.

In the general case, the contribution of phonons to the thermal conductivity coefficient (κ_{ph}) is directly proportional to average phonon velocity v_{ph} and phonon mean-free path l_{ph} [9]: $\kappa_{ph}=C_p v_{ph} l_{ph}/3$ where C_p is the specific heat of the material under consideration. Temperature θ_D is related to the average phonon velocity according to the following equation [30,31]: $\theta_D \sim (2h/\pi k_B)(3N_A/4\pi V_m)^{1/3} v_{ph}$. Here, V_m is the molar volume of the considered material. The dependence of the molar volume on the nanoparticle morphology becomes significant only when the characteristic size of a nanoparticle is 5-10 times lower than the ones regarded in this paper [32], therefore, we obtain $\theta_D^{nano}/\theta_D^{bulk} = v_{ph}^{nano}/v_{ph}^{bulk}$. According to the derivations in [33,34], $l_{ph}^{nano}/l_{ph}^{bulk} = \left(\theta_D^{nano}/\theta_D^{bulk}\right)^2$. After some simple algebraic transformations taking into account all the considerations above, we obtain Eq. (1) for the phonon contribution to the thermal conductivity of a nanoparticle, κ_{ph}^{nano}, as a function of its morphology; κ_{ph}^{bulk} represents the lattice thermal conductivity of the bulk material.

$$\kappa_{ph}^{nano} = \eta \exp\left(1-l_0/d_{eff}\right)\times\left(1-C(\pi/6)^{2/D-1} d_{eff}^{3\left(2/D-5/3\right)} r_{at}\right)\kappa_{ph}^{bulk}. \quad (1)$$

Decreasing the size of nanoparticle and "complicating" its morphology lead to a more significant phonon scattering effect which, in its turn, affects the heat transfer process in nanostructures. A set of models describing the phonon scattering process in nanosystems in different conditions is given in Ref. [35]. In this paper, in order to demonstrate the essence of the phenomenon, we have applied the simple model which has been previously used by M. Goyal [36] (its experimental verification in several cases is also described in [36]). In the framework of this model, we have included pre-term $\eta\exp\left(1-l_{ph}^{bulk}/d_{eff}\right)$ in Eq. (1) where η is the surface roughness parameter, $\eta \in (0,1]$, while ratio l_{ph}^{bulk}/d_{eff} is known as the Knudsen number. According to [36], the larger values of η correspond to a smoother nanoparticle surface leading to a higher probability of the specular scattering and to a lower probability of the diffusive one. Whereas the lower the value of η is, the rougher the surface is, which leads to an increase in the probability of the diffusive scattering resulting in a significant decrease in the lattice thermal conductivity (see Fig. 3).

Note that the correlation between surface roughness η and fractal dimension *D* of a nanoparticle is not unique (since their nature itself is different: the fractal dimension value is associated with the surface-to-volume ratio while the surface roughness corresponds primarily to the number of edges. For example, an *amoeba-like* particle with no edges or an ellipsoid with a high aspect ratio can have fractal dimensions significantly below 3 while their surface roughness parameters can be near to 1). Several notes on the dependence of fractal dimension on the surface roughness are given in [37] (see also their graphical representation in Fig. 2 of [37]). In our considerations, we have varied parameter η from 0.85 up to 1 in increments of 0.05. Without any losses of generality, coefficient *C*, which also matches dimensions, is accepted to be 4π for the sake of convenience. The phonon mean-free path for pure Bi in the bulk state as well as the value of its lattice thermal conductivity have been obtained *ab initio* in [13]. Fig. 3 is plotted for the case the heat transfer takes place in the "*binary*" crystallographic direction ((100)) while the operation temperature of the thermoelectric element is 100 K.

In is also worth mentioning that a high surface-to-volume ratio leading to significant changes in the number of surface atoms as well as in the cohesive energy is characteristic not only to nanoparticles and their ensembles but also for nano- and mesoporous media (see, for examples, our calculations in [38,39]). In such cases, we may expect the dependences of thermal properties on the pore morphology similar to the ones described above. The formation of such structures is possible, for example, during the early stages of spark plasma sintering, laser sintering of nanopowders as well as using a variety of other techniques (see [39] and Refs. therein).

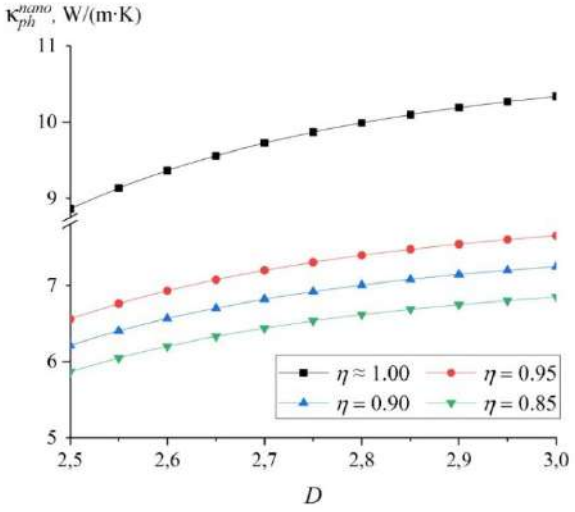

Fig. 3. The dependence of the phonon contribution to the thermal conductivity coefficient on fractal dimension D and surface roughness parameter η for a nanoparticle of pure Bi with d_{eff}=40 nm.

2. Additional remarks on nanoparticle ensembles

In the In the case of nanoparticle ensembles, the average functional properties of particles depend on the size and shape distributions in an ensemble. In [40,41], we have suggested a method for calculating such distributions based on the combined usage of number theory, fractal geometry and statistical thermodynamics. For example, the equilibrium size distributions for nanoparticles with fractal dimension D in a free-dispersed system can be expressed as follows:

$$f_D(\phi_p, D, N):\ \exp\left(-\frac{\gamma A_{sp}(D) + RT\ln f_p}{RT}\right),\ f_p = \frac{N}{N-\phi_p}\exp\left\{\pi\left(\sqrt{\frac{2}{3}}(N-\phi_p) - \sqrt{\frac{2}{3}N}\right)\right\}. \quad (2)$$

Here, $\phi_p = \omega(d_{\text{eff}}/d_{\text{at}})^3$ is the number of atoms in a nanoparticle (its so-called "stoichiometric number"), ω is the lattice packing density, N is the total number of atoms in the system, $A_{sp}(D)$ is the specific surface area of the ensemble, γ is the surface energy of the material in the considered external environment; d_{at} is the atomic diameter. The presented estimates are in perfect accordance with the experimental data (see [40] and Refs. therein) and make it possible to model the thermodynamical conditions for the realization of optimal average geometric characteristics of nanoparticles leading to the optimal thermal and thermoelectric properties as well to predict the degree at which such properties are "blurred" in an ensemble. For example, average fractal dimension $\langle D\rangle$ and average stoichiometric number $\langle\phi_p\rangle$ of nanoparticles in the ensemble can be calculated as follows:

$$\langle D\rangle = \frac{\sum_i D_i \int f_D(D_i,\phi_p,N)\,d\phi_p}{\Omega(N)},\quad \langle\phi_p\rangle = \frac{\sum_i \int \phi_p f_D(D_i,\phi_p,N)\,d\phi_p}{\Omega(N)},\quad \Omega(N) = \sum_i \int f_D(D_i,\phi_p,N)\,d\phi_p. \quad (3)$$

Here, the limits of the integration over ϕ_p belong to range $[1,N]$ while the sample of distributions is considered where $D_i \in (2,3)$ with an arbitrarily selected step.

Similarly, the suggested model makes it possible to determine some other properties of a nanoparticle ensemble, such as effective linear nanoparticle size $\langle l_{eff}\rangle$ (the edge length of the equal-volume cube) or effective nanoparticle diameter d_{eff} (several remarks on the calculation of such values are given in [40]):

$$\langle l_{eff}\rangle = \Omega(N)^{-1} d_{at} \sum_i \int \phi_p^{1/3} f_D(D_i,\phi_p)\,d\phi_p,\quad \langle d_{eff}\rangle = \Omega(N)^{-1} d_{at} \sum_i \int f_D(D_i,\phi_p)\,d\phi_p. \quad (4)$$

It is necessary to note that the numerical calculations of integrals such as $\int x(D_i,\phi_p)\, f_D(D_i,\phi_p)\, d\phi_p$, the upper integration limit being comparable to the Avogadro number, is quite complicated due to the fact the contribution of "huge" particles $\left(\phi_p \in \left[N_A^{0.6}, N_A\right]\right)$ is practically equal to zero. In their standard description, the calculation of such integrals using the software packages such as *Mathworks MathCAD* or *Wolfram Mathematica* can be misleading. In the case *Wolfram Mathematica* is used, the problem can be solved by modifying the integration method as follows: $\left(Method \to \{"DoubleExponential","SymbolicProcessing" \to 0\}\right)$. *Mathworks MathCAD* allows selecting the integration technique: dividing the integration region into the intervals corresponding to the maxima of function $f_D(D_i,\phi_p,N)$ has turned out to be the most appropriate approach.

Wolfram Mathematica allows replacing sum $\sum_i \int x(D_i,\phi_p)\, f_D(D_i,\phi_p,N)\, d\phi_p$ with double integral $\int\int x(D,\phi_p)\, f_D(D,\phi_p,N)\, d\phi_p dD$; in this case, the final result can be obtained through integrating sequentially, at first, over ϕ_p: $X(D,N) = \int x(D_i,\phi_p)\, f_D(D_i,\phi_p,N)\, d\phi_p$, $\phi_p \in [1,N]$; thereafter, over D: $X(N) = \int X(D,N)\, dD$.

Conclusion

Estimating the fractal dimension of nanoparticles using the optical or electron microscopy data can be carried in the framework of various approaches [42]. Among them, it is necessary to mention the so-called "box-counting technique" [43] which allows determining with satisfactory accuracy either the two-dimensional fractal characteristics or the three-dimensional ones using halftone microscopic images. In the two-dimensional case, the technique can be described as follows: the analyzed microscopic image is converted into a monochrome one, the illumination gradient being eliminated and the brightness being normalized if necessary. A mesh is specified over the image with a predetermined step, and then the image is transformed into a binary matrix where "1" corresponds to the mesh cells with the brightness above the specified threshold value. "0" corresponds to the others. Fractal dimension D is estimated according to the following dependence: $S \sim L^D$ (to within a dimensional factor) where S is the area of the "white" surface (equal to the number of coloured mesh cells) while L is the linear size of the image (matrix rank) [44]. It is worth mentioning that the value of fractal dimension D is sensitive to the chosen brightness threshold, P, in the most general case. For the well-founded selection of the value of P as well as for the elimination of possible ambiguations, the calibration dependence, $D(P)$, is constructed; the example of such dependence is given in [46]. In the three-dimensional case, a 3D mesh is specified where two axes correspond to the spatial coordinates while the third one stands for different levels of the image brightness. The fractal dimension is determined using the relation between the number of cells with the brightness above the specified threshold and the total number of cells. For each cell with a high brightness value, all the cells below are also taken into account.

Acknowledgments

The authors cordially thank Mikhail V. Dorokhin for useful discussions and providing valuable remarks.

REFERENCES

1 Rowe D.M. (ed.) *Thermoelectric handbook macro to nano*. Boca Raton, CRC Press. 2006. 1008 p.

2 Tambasov I.A., Voronin A.S., Evsevskaya N.P., et al. Thermoelectric properties of low-cost cost transparent single wall carbon nanotube thin films obtained by vacuum filtration. *Phys E*. 2019. Vol. 114. 113619. https://doi.org/10.1016/j.physe.2019.113619.

3 Hu J.-Z., Liu B., Zhou J., et al. Enhanced thermoelectric cooling performance with graded thermoelectric materials. *Jpn. j. appl. phys*. 2018. Vol. 57, pp. 71801 – 71806. www.doi.org/10.7567/JJAP.57.071801.

4 Li Z., Miao N., Zhou J., et al. High thermoelectric performance of few-quintuple Sb_2Te_3 nanofilms. *Nano energy*. 2018. Vol. 43, pp. 285 – 290. www.doi.org/10.1016/j.nanoen.2017.11.043.

5 Erofeeva I.V., Dorokhin M.V., Lesnikov V.P., et al. Thermoelectric effects in nanoscale layers of manganese silicide. *Semiconductors*. 2017. Vol. 51, No. 11, pp. 1403 – 1408. www.doi.org/10.1134/S1063782617110112.

6 Caballero-Calero O., Martín-González M. Thermoelectric nanowires: A brief prospective.*Scripta mater*. 2016. Vol. 111, pp. 54 – 57. www.doi.org/10.1016/j.scriptamat.2015.04.020.

7 Dorokhin M.V., Erofeeva I.V., Kuznetsov Yu.M., et al. Investigation of the initial stages of spark-plasma siltering of Si-Ge-based thermoelectric materials. *Nanosyst.: phys., chem., math*. 2018. Vol. 9, No. 5, pp. 622 – 630. www.doi.org/10.17586/2220-8054-2018-9-5-622-630.

8 Kuznetsov Yu.M., Bastrakova M., Dorokhin M.V., et al. Molecular dynamics studies on spark-plasma sintering of Si-Ge-based thermoelectric materials. *AIP adv*. 2020. Vol.10, No.6, 065219. https://doi.org/10.1063/5.0011740.

9 Bulat L.P., Drabkin I.A., Karatayev V.V., et al. Effect of boundary scattering on the thermal conductivity of a nanosctructured semiconductor material based on the $Bi_xSb_{2-x}Te_3$ solid solution. *Phys. solid state*. 2010. Vol. 52, No. 9, pp. 1836 – 1841. https://doi.org/10.1134/S1063783410090088.

10 Shishulin A.V., Fedoseev V.B., Shishulina A.V. Phonon thermal conductivity and phase equilibria of fractal Bi-Sb nanoparticles. *Tech. phys.* 2019. Vol. 64, No. 4, pp. 512 – 517. www.doi.org/10.1134/S1063784219040200.

11 Shishulin A.V., Potapov A.A., Shishulina A.V. *Fractal nanoparticles of phase-separating solid solutions: nanoscale effects on phase equilibria, thermal conductivity, thermoelectric performance*. 14th Chaotic modeling and simulation, Springer proceedings in complexity. www.doi.org/10.1007/978-3-030-96964-6_30.

12 Fedoseev V.B., Shishulin A.V. Shape effect in layering of solid solutions in small volume: bismuth-antimony alloy. *Phys. solid state*. 2018. Vol. 60, No. 7, pp. 1398 – 1404. www.doi.org/10.1134/S1063783418070120.

13 Lee S., Esfarjani K., Mendoza J., et al. Lattice thermal conductivity of Bi, Sb, and Bi-Sb alloy from first principles. *Phys. rev. B*. 2014. Vol. 89, pp. 85206 – 85215. www.doi.org/10.1103/PhysRevB.89.085206.

14 Shishulin A.V., Fedoseev V.B.Stratifying polymer solutions in microsized pores: phase transitions induced by deformation of a porous material. *Tech. phys*. 2020. Vol.65, No.3, pp. 340 – 346. www.doi.org/10.1134/S1063784220030238.

15 Shishulin A.V., Fedoseev V.B. Thermal stability and phase composition of stratifying polymer solutions in small-volume droplets. *J. eng. phys. thermophys*. 2020. Vol. 93, No. 4, pp. 802 – 809. www.doi.org/10.1007/s10891-020-02182-9.

16 Shishulin A.V., Fedoseev V.B.Features of the influence of the initial composition of organic stratifying mixtures in microsized pores on the mutual solubility of components. *Tech. phys. lett.* 2020. Vol. 46, No. 9, pp. 938 – 941. www.doi.org/10.1134/S1063785020090291.

17 Geoffrion L.-D., Guisbiers G. Chemical ordering in $Bi_{1-x}Sb_x$ nanostructures: alloy, janus or core-shell. *J. phys. chem. C*. 2020. Vol. 124, No.25, pp. 14061 – 14068. www.doi.org/10.1021/acs.jpcc.0c04356.

18 Guisbiers G. Advances in thermodynamic modeling of nanoparticles. *Adv. phys. X*. 2019. Vol. 4, No. 1, 1668299. www.doi.org/10.1080/23746149.2019.1668299

19 Hill T.L. *Thermodynamics of small systems. Parts 1 & 2*. Mineola, New York, Dover Publications. 2013. 416 p.

20 Qi W.H., Wang M.P. Size and shape-dependent melting temperature of metallic nanoparticles. *Mater. chem. phys*. 2004. Vol. 88, pp. 280 – 284. www.doi.org/10.1016/j.matchemphys.2004.04.026.

21 Rose J.H., Ferrante J., Smith J.R. Universal features of bonding in metals. *Phys. rev. B*. 1983. Vol. 28, No. 4, pp. 1835 – 1845. https://doi.org/10.1103/PhysRevB.28.1835.

22 Guinea F., Rose J.H., Smith J.R. et al. Scaling relations in the equation of state, thermal expansion and melting of metals. *Appl. phys. lett*. 1984. Vol. 44, pp. 53 – 55. https://doi.org/10.1063/1.94549.

23 Fedoseev V.B., Potapov A.A., Shishulin A.V., Fedoseeva E.N. Size and shape effect on the phase transitions in a small system with fractal interphase boundaries. *Eurasian phys. tech. j*. 2017. Vol. 14, No.1, pp. 18 – 24.

24 Shishulin A.V., Fedoseev V.B. Peculiarities of phase transformations of polymer solutions in deformable porous matrices. *Tech. phys. lett*. 2019. Vol. 45, No. 7, pp. 697 – 699. https://doi.org/10.1134/S1063785019070289.

25 Potapov A.A. On fractal dimension spectrum of new lightning discharge types in ionosphere: elves, jets and sprites. *Eurasian phys. tech. j*. 2016. Vol. 13, No. 2, pp. 5 – 11.

26 Shishulin A.V., Fedoseev V.B. On some peculiarities of stratification of liquid solutions within pores of fractal shape. *J. mol. liq*. 2019. Vol. 278, pp. 363 – 367. www.doi.org/10.1016/j.molliq.2019.01.050.

27 Shishulin A.V., Fedoseev V.B., Shishulina A.V. Melting behavior of fractal-shaped nanoparticles (the example of Si-Ge system). *Tech. phys*. 2019. Vol. 64, No. 9, pp. 1343 – 1349. https://doi.org/10.1134/S1063784219090172.

28 Potapov A.A. On the issues of fractal radio electronics: Processing of multidimensional signals, radiolocation, nanotechnology, radio engineering elements and sensors. *Eurasian phys. tech. j*. 2018. Vol. 15, No. 2, pp. 5 – 15.

29 Vopson M.M., Rogers N., Hepburn I. The generalized Lindemann melting coefficient. *Solid state commun*. 2020. Vol. 218. 113977. www.doi.org/10.1016/j.ssc.2020.113977.

30 Post E.J. On the characteristic temperatures of single crystals and the dispersion of "Debye heat waves". *Can. j. phys*. 1953. Vol. 31, No. 1, pp. 112 – 119. https://doi.org/10.1139/p53-010.

31 Regal A.R., Glazov V.M. Entropy of melting of semiconductors. *Semiconductors*. 1995. Vol. 29, No. 5, pp. 405 – 417.

32 Magomedov M.N. On the statistical thermodynamics of a free-standing nanocrystal: silicon. *Cryst. rep*. 2017. Vol. 63, No. 3, 480 – 496. https://doi.org/10.1134/S1063774517030142.

33 Zimann J.M. *Electrons and phonons*. Oxford, Clarendon Press. 1960. pp. 58, 288, 396, 456.

34 Soyez G., Eastman J.A., Thompson L.J. et al. Grain-size-dependent thermal conductivity of nanocrystalline yttria-stabilized zirconia films grown by metal-organic chemical vapor deposition. *Appl. phys. lett*. 2000. Vol. 77, No. 8, pp. 1155 – 1157. https://doi.org/10.1063/1.1289803.

35 Khvesyuk V.I. Skryabin A.S. Heat conduction in nanostructures. *High temp*. 2017. Vol. 55, No. 3, pp. 434 – 456. https://doi.org/10.1134/S0018151X17030129.

36 Goyal M. Shape, size and phonon scattering effect on the thermal conductivity of nanostructures. *Pramana: j. phys.* 2018. Vol. 91, pp.87. www.doi.org/10.1007/s12043-018-1660-8.

37 Fedoseev V.B. The use of fractal geometry for the thermodynamic description of the free-dimensional crystal structure elements. *Lett. mater*. 2012. Vol. 2, pp. 78 – 83.

38 Shishulin A.V., Fedoseev V.B., Shishulina A.V. Variation of the Curie temperature in porous materials. *Tech. phys. lett*. 2020. Vol. 46, No. 7, pp. 680 – 682. https://doi.org/10.1134/S106378502007024X.

39 Shishulin A.V., Potapov A.A., Shishulina A.V. On the transition between ferromagnetic and paramagnetic states in mesoporous materials with fractal morphology. *Eurasian phys. tech. j.* 2021. Vol. 18, No.2, pp. 6 – 11. https://doi.org/10.31489/2021NO2/6-11.

40 Fedoseev V.B., Shishulin A.V. On the size distribution of dispersed fractal particles. *Tech. phys*. 2021. Vol. 66, No. 1, pp. 34 – 40. www.doi.org/10.1134/S1063784221010072.

41 Shishulin A.V., Potapov A.A., Shishulina A.V. The initial composition as an additional parameter determining the melting behavior of nanoparticles (a case study on Si_x-Ge_{1-x} alloys). *Eurasian phys. tech. j.* 2021. Vol. 18, No.4, pp. 5 – 13. https://doi.org/10.31489/2021NO4/5-14.

42 Potapov A.A., Pakhomov A.A., Potapov A.A. (Jr.), Potapov V.A. Processing by robust fractal-topological methods of flows of optical texture images on the Martian surface. *Eurasian phys. tech. j*. 2019. Vol. 16, No.2, pp. 5 – 10. https://doi.org/10.31489/2019NO2/5-10.

43 Li J., Du Q., Sun C. An improved box-counting method for image fractal dimension estimation *Pattern recognit*. 2009. Vol. 42, pp. 2460 – 2469. www.doi.org/10.1016/j.patcog.2009.03.001.

44 Fedoseeva E.N., Fedoseev V.B. Interaction of chitosan with benzoic acid in solution and films. *Polymer sci. Ser. A.* 2011. Vol. 53, No. 11, pp. 1040 – 1046. https://doi.org/10.1134/S0965545X1110004X.

Article accepted for publication 27.06.2022